Rare Met.
https://doi.org/10.1007/s12598-022-02171-2

RARE METALS

LETTER

Ultrasonic vibration-assisted multi-scale plastic forming of high-entropy alloys in milliseconds

Wen-Xin Wen, Lu-Yao Li, Zhen Li, Wen-Qing Ruan, Shuai Ren, Zhen-Xuan Zhang, Xiong Liang, Huan Liu*, Jiang Ma*

Received: 25 June 2022 / Revised: 28 July 2022 / Accepted: 29 July 2022

Due to their excellent properties of specific strength, fracture resistance, corrosion and oxidation resistance, the high-entropy alloys have attracted widespread attention as engineering materials. For the sake of industrial applications, one of the essential stages would be the forming of them, especially the construction of multi-scale structures from macroscale to nanoscale. In this work, an efficient method to achieve the fabrication of multi-scale structures on the high-entropy alloys is proposed, namely ultrasonic vibration-assisted plastic forming. In this way, the required pressure can be effectively reduced from 1.53 GPa to 6.87 MPa. And the whole process takes place in milliseconds. Meanwhile, transmission electron microscopy (TEM) and electron backscatter diffraction (EBSD) were used to explore the plastic deformation mechanisms of a synergy between dislocation and twinning. The current findings open a window not only to propose new methods for forming multi-scale structures of high-entropy alloys but also to reveal the plastic deformation mechanism.

W.-X. Wen, L.-Y. Li, W.-Q. Ruan, S. Ren, Z.-X. Zhang, X. Liang, J. Ma*
Shenzhen Key Laboratory of High Performance Nontraditional Manufacturing, College of Mechatronics and Control Engineering, Shenzhen University, Shenzhen 518060, China
e-mail: majiang@szu.edu.cn

Z. Li
Department of Mechanics and Aerospace Engineering, Southern University of Science and Technology, Shenzhen 518055, China

H. Liu*
College of Mechanics and Materials, Hohai University, Nanjing 210000, China
e-mail: liuhuanseu@hhu.edu.cn

Ultrasonic processing is a non-traditional machining method which uses ultrasonic vibration to introduce energy into the machining process. It mainly relies on the instantaneous local impact of abrasive to remove the machined material, and the macroscale cutting force and cutting heat in the whole process are very small. Therefore, the tool load is reduced, the workpiece is less prone to surface burns, and the degree of surface finish is improved, further improving machining quality and efficiency [1–4]. At the same time, it is especially suitable for processing parts with thin wall [5], micro-groove [6] and low stiffness [7].

In 1955, Blaha and Langenecker [8] found a sudden reduction in the deformation force of materials under ultrasonic vibration. Subsequently, in 1966, Langenecker [9] proposed that ultrasonic vibration could soften metals without heating. This phenomenon is now often referred to as acoustoplasticity. Based on this interesting property, scientists have conducted numerous studies in terms of volume effects and surface effects [10, 11]. Dislocation theory as a representative of volume effects is considered to preferentially absorb acoustic energy and thus reduce critical stress [9, 12]. Likewise, friction has become a frequent subject of discussion on the surface effects of ultrasonic vibration [13]. Based on this unique property and scientists' research on the mechanism, ultrasonic vibration-assisted plastic forming (UAPF) was born. In industry, this technology is used in engineering applications for plastic processing processes such as piercing [14], injection molding [15], powder molding [16], wire drawing [17], extrusion [18], sheet molding [19].

With the further study of materials, multi-principal element alloys have gradually become a new hot spot in the field of metallurgy. They include medium-entropy alloys (MEAs) and high-entropy alloys (HEAs). MEAs are usually ternary systems with good mechanical properties. For

Published online: 01 December 2022

instance, CrCoNi-based MEAs have excellent strength-toughness properties, strength and ductility at cryogenic temperatures and high strain rates [20–22]. HEAs with good fracture toughness [23], tensile strength [24], corrosion resistance [25], oxidation resistance [26] and other excellent properties are gradually on the stage of engineering materials. It is well known that HEAs have four unique effects: high-entropy effect [27], sluggish diffusion effect [28], "cocktail" effect [29] and lattice distortion effect [30]. Although scientists have conducted some research on HEAs, little research has been done on the formation of microscale and nanoscale structures of HEAs. On the one hand, scientists have only studied some aspects of processing such as the ultra-precision cutting [31] or ultrasonic vibration-assisted turning [32] of HEAs. On the other hand, existing processing methods such as additive manufacturing for structural forming require expensive equipment, a long manufacturing cycle and restricted ultimate forming dimensions [33, 34].

Therefore, this work proposes a more convenient method for the forming of HEAs, that is, UAPF of HEAs at macro- to nanoscale. Ultrasonic vibration not only prevents the dislocation from plugging at the grain boundary during UAPF but also induces the formation of twins. This allows dislocations and twins to absorb more energy, leading to the continuation of plastic deformation. That is to say, UAPF can be used to widen the limit size of structures. Due to the mechanical effect of ultrasonic processing, the pressure required for material forming can be effectively reduced from 1.53 GPa to 6.87 MPa. Moreover, due to the rapid release of ultrasonic vibration, the whole time of UAPF is usually in milliseconds, so it makes the processing very efficient. In tests, the temperature rise of the whole process is less than 100 K and can be restored to room temperature after 15 s. The UAPF method will provide a better scheme for the rapid plastic forming of HEAs.

The CoCrFeNiMn HEAs were prepared from five elements with a purity of 99 at% by vacuum arc melting. Then, the samples were cut to 20 mm in length, 8 mm in width and 3 mm in height using wire electrical discharge machining-low speed (WEDM-LS). Samples with a diameter of 5 mm and a height of 2 mm, and a diameter of 4 mm and a height of 1 mm were also prepared by WEDM-LS. The surface of the samples was then polished with a polishing machine using 400, 800, 1200, 1500 and 2000 meshes abrasive papers and velvet polishing cloth, respectively.

The whole process consisted of generating a high voltage, high-frequency signal of 20 kHz from the generator and converting the signal into high-frequency mechanical vibration through the transducer system, and then contacting by the ultrasonic indenter (Ti-6Al-4V) to the sample. Due to the short working cycle, the total vibration time can be controlled in milliseconds.

The low-magnification structures were observed by scanning electron microscopy (SEM; Quanta FEG 450, FEI, America). Through the confocal laser scanning microscope (CLSM; VK250, KEYENCE, Japan), the three-dimensional morphology and dimensional data of the molds and HEAs could be obtained. In order to further observe the evolution of microstructure and thus speculate on the mechanism, the HEA samples were prepared by SEM/focused ion beam (FIB) double beam system (FEI SCIOS, FEI, America). The microstructure was then analyzed by a double spherical aberration corrected transmission electron microscope (TEM; FEI Titan Cubed Themis G2 300, FEI, Netherlands). The characteristics of the microstructure were observed by the high-angle annular dark field (HAADF) and selected area electron diffraction (SAED) patterns, and the TEM-equipped energy-dispersive spectroscopy (EDS) was used to analyze the surface element distribution. Besides, through EBSD equipped with an HKL-EBSD system, the microstructural features of the sample deformation zone were characterized using the field emission scanning electron microscope (FESEM; MAIA3, TESCAN, Czech). The samples were prepared by ion-beam polishing for 1 h at 6.5 kV, and the EBSD characterizations were operated with a step size of 0.5–2 μm at 20 kV. Eight points were selected from the untreated samples and the UAPF-treated samples, respectively, to obtain the changes in the mechanical properties of HEA. Then, the surface hardness was then measured at the selected location under a load of 4.90 N for 10 s with the automatic Vickers hardness tester. Load measurement was performed using a self-made dynamometer, and a data-acquisition card (National Instruments NI-9237) with a sampling frequency of 500 Hz was used to transmit the data to a computer. The thermal images were captured by the infrared imaging camera (Fotric 280d, FOTRIC, China) with a sampling frequency of 60 Hz.

Figure 1a shows schematic diagram of UAPF. The whole process of UAPF is very simple, i.e., the HEA and the mold are stacked in a locating part, and then, ultrasonic vibration is applied to them by the indenter. Macroscale structures can be prepared in this simple way. Figure 1b shows a mold with the structure of the convex "HEA" letters, and Fig. 1c shows a HEA replica sample with the structure of Fig. 1b. CLSM images with blue and red square areas in Fig. 1d correspond to the positions in Fig. 1b and c and show the flatness of the replicated structures. Besides, HEA can also replicate the concave structure of the mold. Figure 1e corresponds to a mold with the structure of the concave "HEA" letters, and Fig. 1f shows a sample of HEA with a replica of the structure in Fig. 1e. Similarly, the CLSM image with orange and yellow square areas in Fig. 1g corresponds to the positions in Fig. 1e and f, showing the flatness of the replication

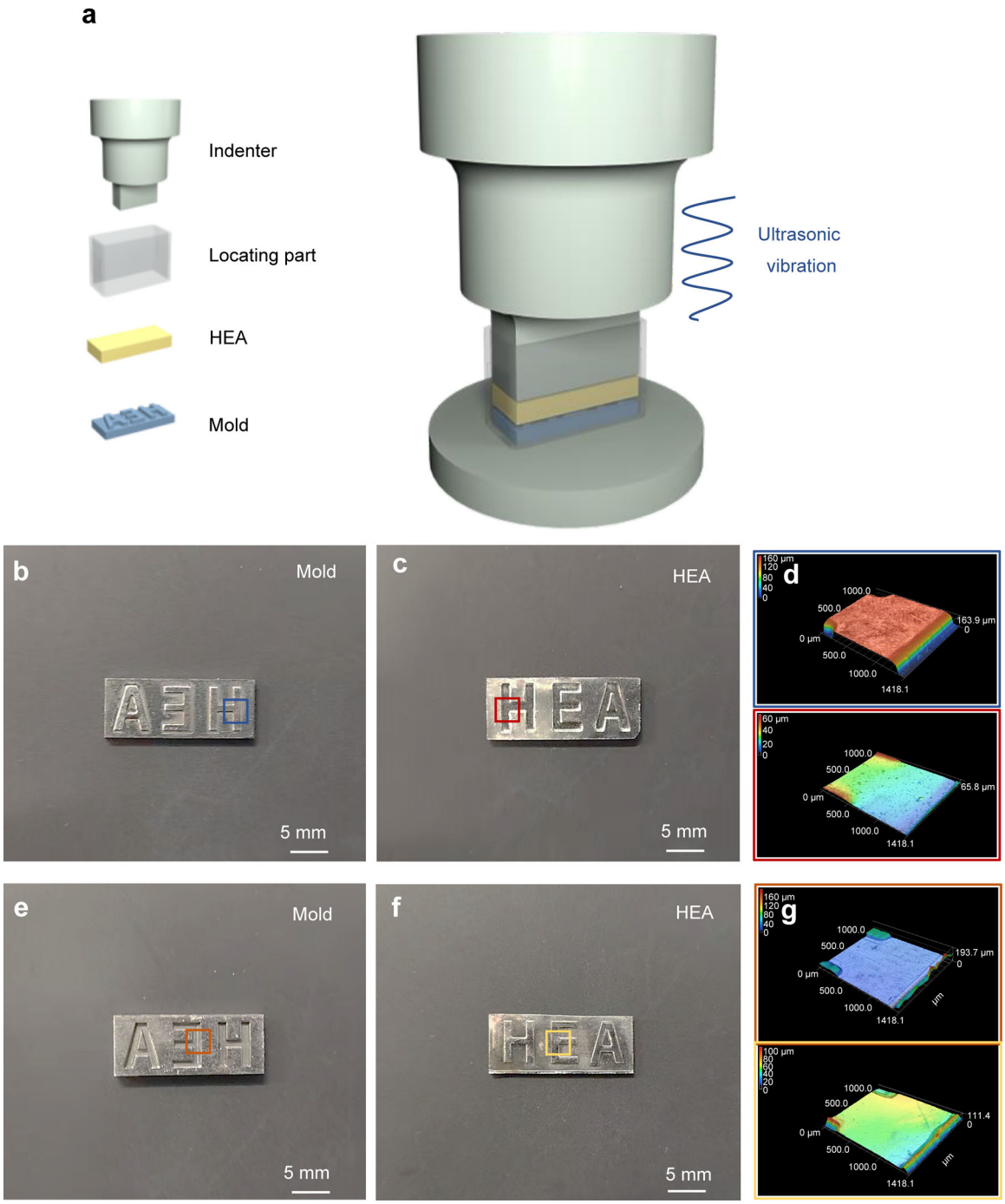

Fig. 1 **a** Schematic diagram of UAPF; **b** mold of a structure with a convex structure of "HEA" letters; **c** reproduction of HEA sample with the structure of **b**; **d** CLSM images represent flatness of blue and red square areas in **b** and **c**; **e** mold of a structure with a concave structure of "HEA" letters; **f** reproduction of HEA sample with structure of **e**; **g** CLSM images represent flatness of orange and yellow square areas in **e** and **f**

structure. It can be seen that macrostructures can be prepared by UAPF with good replication accuracy and quality.

Through UAPF, the microscale and nanoscale structures of HEAs can also be prepared. Figure 2a shows the HEA sample with microgrooves, and it is prepared by the structures of the stainless steel mold in Fig. 2b. Figure 2c shows a cross-groove structure prepared by the tungsten carbide mold in Fig. 2d. In addition, 200 nm diameter nanowires and 390 nm nanowires can also be prepared by UAPF in Fig. 2e and f. Figure 2g shows the lateral morphology of the 200 nm nanowires. These microstructures allow HEAs to have more potential applications.

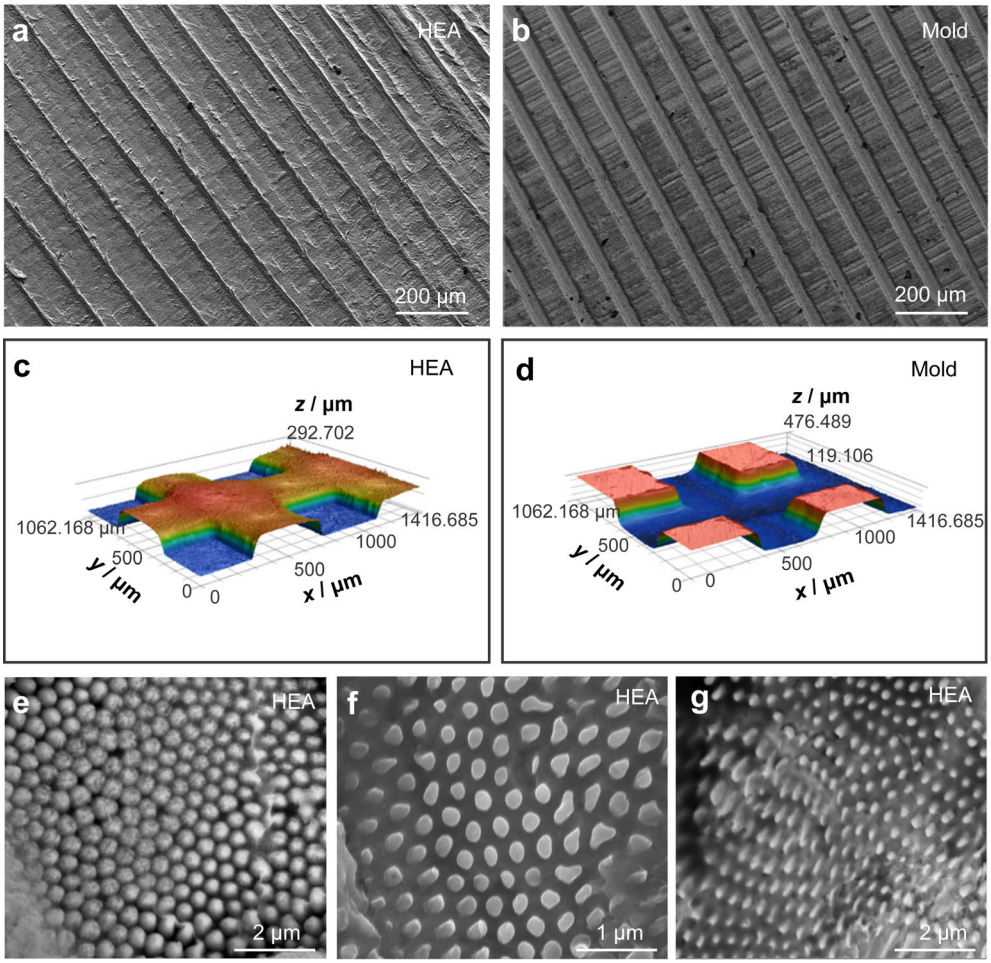

Fig. 2 **a** SEM image of reproduction of HEA sample with straight groove structure; **b** SEM image of straight groove structure in mold; **c** CLSM image of reproduction of HEA sample with cross-groove structure; **d** CLSM image of cross-groove structure in mold; SEM image showing HEA nanowire prepared using anodic aluminum oxide (AAO) template of **e** 200 nm, **f** 390 nm; **g** SEM image showing lateral morphology of 200 nm diameter nanowires

To further investigate the mechanism of UAPF action on HEAs, the microstructures of as-cast HEA and the UAPF-treated samples were observed. In contrast with the atomic arrangement in HRTEM image of as-cast HEA in Fig. 3a, the UAPF-treated sample in Fig. 3b shows a sea of defects. Figure 3c shows the one-dimensional Fourier-filtered image of Fig. 3b, showing a set of planes with blue arrows. The dislocations are displayed in the form of symbols ⊥ in Fig. 3c. As shown in Fig. 3d, the green lines in EBSD image represent the grain boundaries of adjacent grains whose phase difference is less than 10°, known as low-angle grain boundaries. Low-angle grain boundaries can be considered as arrays of dislocations [35]. Figure 3e shows the large-scale morphology of the UAPF-treated sample under TEM. By the difference of the contrast, the position of the dark color can be analyzed as the area with dense dislocations. Not only that, but also obvious stacking faults (SFs) and deformation twins (DTs) were observed in the region of high-density defects. Figure 3f and h shows both HRTEM images, and their enlargements are in Fig. 3g and i, respectively, both reflecting the distinctive features of SFs. Even more, multiple deformation twins were found in the other region of high-density defects, as shown in Fig. 3j. Figure 3k represents HRTEM image of the green square area in Fig. 3j. The characteristics of the multiple deformation twins can be further confirmed by fast Fourier transform (FFT) image in Fig. 3l. EDS equipped in TEM is used to map elemental distributions. As shown in Fig. 3m, it does not show appreciable compositional variations in the area with many defects.

The deformation mode of high-entropy alloys under dynamic loading is dislocation based, and dislocations rapidly increase in value and generate dislocation entanglement at high strain rates [36]. As the plastic deformation of the metal continues, slip within the crystal becomes difficult. At this time, twinning can coordinate the stress–

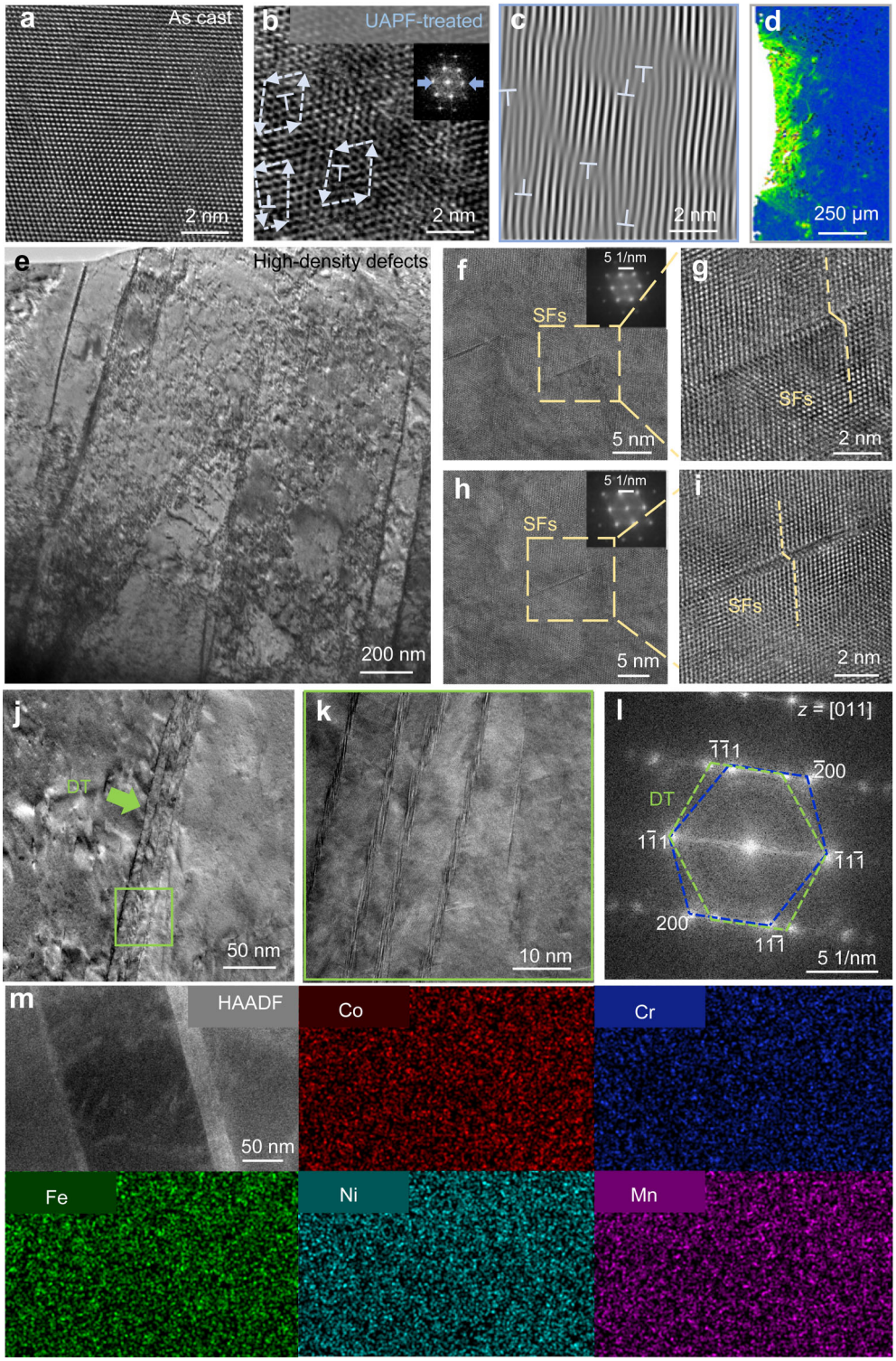

Fig. 3 **a** HRTEM image of as-cast HEA sample; **b** HRTEM image of UAPF-treated HEA sample; **c** one-dimensional Fourier-filtered image of **b**, showing a set of planes with blue arrows. Dislocations are displayed in the form of symbols ⊥; **d** EBSD image of local misorientation showing dislocation density; **e** low-magnification TEM image showing high-density defects; **f** HRTEM image showing SFs; **g** HRTEM image taken from the yellow square area in **f**; **h** HRTEM image showing SFs; **i** HRTEM image taken from yellow square area in **h**; **j** TEM image showing multiple DTs; **k** HRTEM image taken from green square area in **j**; **l** FFT image of **k** showing DT feature; **m** EDS images showing elemental distribution

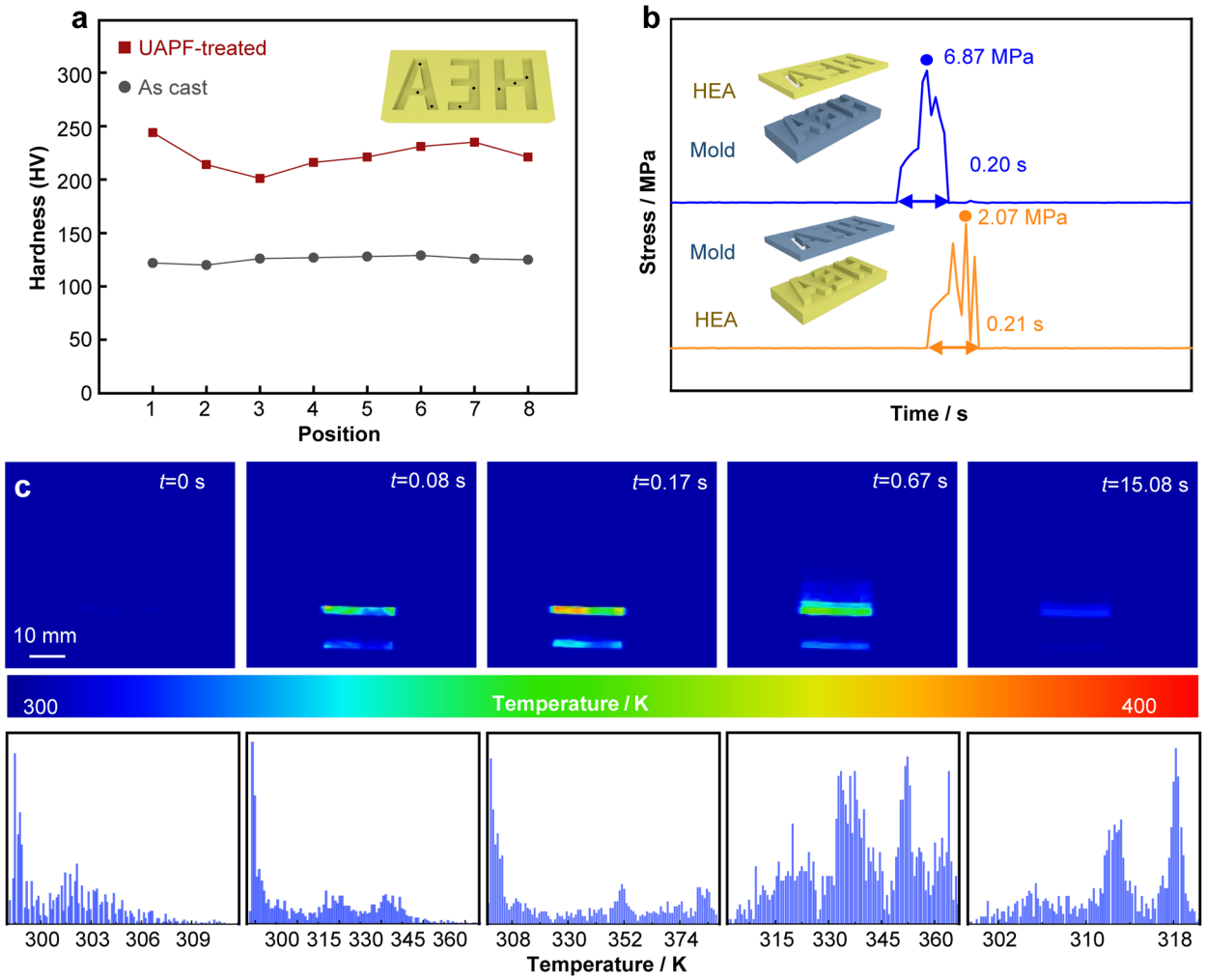

Fig. 4 **a** Comparison of hardness of as-cast HEA and UAPF-treated HEA; **b** time–stress curve of convex structure and concave structure forming process; **c** temperature distribution image and temperature numerical distribution

strain and ensure a certain degree of plastic deformation capacity. The formation of twins will change the orientation of the crystals and induce the transformation of certain non-easy slip systems to easy slip systems, and subsequently, the opening of new slip systems will promote the multiple slip of dislocations [37]. Moreover, multiple twins can provide easy dislocation slip and cross-slip paths while creating greater barriers to dislocations [38]. At the same time, the instantaneous stress provided by dynamic loading will change the twin threshold of HEAs [39]. Twins play an important role in the dynamic deformation of HEAs with low fault energy. Because the instantaneous stress under dynamic load brought by high-frequency ultrasonic vibration is very high, twinning is more easily induced [40]. As is known to all, CoCrFeNiMn HEA has low stacking fault energy, resulting in a more likely occurrence of twins [41, 42]. That is to say, the HEAs of lower fault energy are easy to coordinate plastic deformation by twinning. Coincidentally, researchers have also shown that through ultrasonic vibration, the compression strain of $Al_{80}Li_5Mg_5Zn_5Cu_5$ entropic alloy increases from 17% under conventional compression to 30%, while the applied stress is less than 100 MPa [43].

According to EBSD and TEM figures above, many low-angle grain boundaries and twinning boundaries can be observed, leading to the occurrence of grain boundary strengthening [44]. At the same time, in the process of deformation, ultrasonic vibration can refine the grains of metals [43], increase the area of grain boundary per unit volume and realize strengthening. As shown in Fig. 4a, it is obvious that the Vickers hardness has increased to twice the original hardness.

Also, the UAPF process conditions are friendly to material forming. As shown in Fig. 4b, when a convex mold is used to form a concave structure, a pressure of 6.87 MPa and a very short time of 0.20 s are generally required. Similarly, when a concave mold is used to form a convex structure, a pressure of 2.07 MPa and a time of 0.21 s are required.

Compared to the previous cold embossing work on HEAs where the minimum required pressure was 1.53 GPa, this work even requires the pressure of 6.87 MPa [45]. Moreover, although the previous work already had a short molding time of 7 s, this work can be molded in milliseconds [45]. This makes the forming of HEAs efficient. At the same time, the temperature rise of the UAPF process is not obvious. The maximum temperature of the HEAs throughout the UAPF process was 389.15 K and returned to near room temperature after 15 s. Figure 4c shows the temperature distribution at some time points during the UAPF process and no high temperature was generated during the process. This can, to a certain extent, reduce the adverse effects of the warming effect on the mechanical properties and physical properties of the material.

In this work, an efficient method was developed to prepare the multi-scale structures on CoCrFeNiMn HEA in milliseconds. Through the UAPF method, the macroscale structures with "HEA" letter structures, microscale groove structures and nanoscale nanowire structures can be easily prepared. At the same time, due to dislocation plug and high-frequency vibration, twin coordinated plastic deformation occurs. Therefore, plastic deformation can continue and further improve the forming limit size of the material to achieve the forming of a more macroscopic structure. Due to fine grain strengthening and grain boundary strengthening, HEA samples are twice as strong as untreated samples after UAPF. Not only that, due to ultrasonic vibration in the forming process, the pressure is significantly reduced and only needs less than 10 MPa. As the temperature does not increase significantly during the process, the adverse effects easily brought about by the warming effect are suppressed. All of these make UAPF easy to be industrialized due to its simple processing conditions, fast forming speed in milliseconds and high quality.

Acknowledgements The work was financially supported by the National Key Research and Development Program of China (Nos. 2018YFA0703605), the Key Basic and Applied Research Program of Guangdong Province, China (No. 2019B030302010), the National Natural Science Foundation of China (Nos. 52122105, 51971150 and 51871157). The authors thank the assistance on microscope observation received from the Electron Microscope Center of Shenzhen University.

Declarations

Conflict of interests The authors declare that they have no conflict of interest.

References

[1] Liu JT, Kang RK, Dong ZG, Zheng FF, Zeng YF, Bao Y. Experimental investigation of damage formation and material removal in ultrasonic assisted grinding of RBSiC. Mater Res Express. 2020;7(12):125202. https://doi.org/10.1088/2053-1591/abd069.

[2] Sui H, Zhang XY, Zhang DY, Jiang XG, Wu RB. Feasibility study of high-speed ultrasonic vibration cutting titanium alloy. J Mater Process Technol. 2017;247:111. https://doi.org/10.1016/j.jmatprotec.2017.03.017.

[3] Yang ZC, Zhu LD, Lin B, Zhang GX, Ni CB, Sui TY. The grinding force modeling and experimental study of ZrO_2 ceramic materials in ultrasonic vibration assisted grinding. Ceram Int. 2019;45(7):8873. https://doi.org/10.1016/j.ceramint.2019.01.216.

[4] Shen JY, Zhu X, Chen JB, Tao P, Wu X. Investigation on the edge chipping in ultrasonic assisted sawing of monocrystalline silicon. Micromachines. 2019;10(9):616. https://doi.org/10.3390/mi10090616.

[5] Gao GF, Zhao B, Jiao F, Liu CS. Research on the influence of the cutting conditions on the surface microstructure of ultra-thin wall parts in ultrasonic vibration cutting. J Mater Process Technol. 2002;129(1–3):66. https://doi.org/10.1016/S0924-0136(02)00577-0.

[6] Zhang C, Guo P, Ehmann KF, Li YG. Effects of ultrasonic vibrations in micro-groove turning. Ultrasonics. 2016;67:30. https://doi.org/10.1016/j.ultras.2015.12.016.

[7] Tong JL, Wei G, Zhao L, Wang XL, Ma JJ. Surface microstructure of titanium alloy thin-walled parts at ultrasonic vibration-assisted milling. Int J Adv Manuf Technol. 2019;101(1):1007. https://doi.org/10.1007/s00170-018-3005-7.

[8] Blaha F, Langenecker B. Tensile deformation of zinc crystal under ultrasonic vibration. Naturwissenschaften. 1955;42(556):1.

[9] Langenecker B. Effects of ultrasound on deformation characteristics of metals. IEEE Trans Sonics Ultrason. 1966;13(1):1. https://doi.org/10.1109/T-SU.1966.29367.

[10] Hu J, Shimizu T, Yang M. Investigation on ultrasonic volume effects: stress superposition, acoustic softening and dynamic impact. Ultrason Sonochem. 2018;48:240. https://doi.org/10.1016/j.ultsonch.2018.05.039.

[11] Storck H, Littmann W, Wallaschek J, Mracek M. The effect of friction reduction in presence of ultrasonic vibrations and its relevance to travelling wave ultrasonic motors. Ultrasonics. 2002;40(1–8):379. https://doi.org/10.1016/S0041-624X(02)00126-9.

[12] Lum I, Huang H, Chang BH, Mayer M, Du D, Zhou Y. Effects of superimposed ultrasound on deformation of gold. J Appl Phys. 2009;105(2): 024905. https://doi.org/10.1063/1.3068352.

[13] Daud Y, Lucas M, Huang ZH. Modelling the effects of superimposed ultrasonic vibrations on tension and compression tests of aluminium. J Mater Process Technol. 2007;186(1–3):179. https://doi.org/10.1016/j.jmatprotec.2006.12.032.

[14] Mita K, Hu J, Shimizu T, Yang M. Shearing characteristics in ultrasonic vibration-assisted piercing of fine-grained stainless steel foils. Procedia Manuf. 2018;15:627. https://doi.org/10.1016/j.promfg.2018.07.287.

[15] Sánchez-Sánchez X, Hernández-Avila M, Elizalde LE, Martínez O, Ferrer I, Elías-Zuñiga A. Micro injection molding processing of UHMWPE using ultrasonic vibration energy. Mater Des. 2017;132:1. https://doi.org/10.1016/j.matdes.2017.06.055.

[16] Zeng K, Wu XY, Liang X, Xu B, Wang YT, Chen XQ, Cheng R, Luo F. Process and properties of micro-ultrasonic powder molding with polypropylene. Int J Adv Manuf Technol. 2014;70(1–4):515. https://doi.org/10.1007/s00170-013-5300-7.

[17] Liu S, Shan XB, Guo K, Yang YC, Xie T. Experimental study on titanium wire drawing with ultrasonic vibration. Ultrasonics. 2018;83:60. https://doi.org/10.1016/j.ultras.2017.08.003.

[18] Bunget C, Ngaile G. Influence of ultrasonic vibration on micro-extrusion. Ultrasonics. 2011;51(5):606. https://doi.org/10.1016/j.ultras.2011.01.001.

[19] Zhai WD, Li YL, Cheng ZN, Sun LL, Li FY, Li JF. Investigation on the forming force and surface quality during ultrasonic-assisted incremental sheet forming process. Int J Adv Manuf Technol. 2020;106(7–8):2703. https://doi.org/10.1007/s00170-019-04870-0.
[20] Gludovatz B, Hohenwarter A, Thurston KV, Bei HB, Wu ZG, George EP, Ritchie RO. Exceptional damage-tolerance of a medium-entropy alloy CrCoNi at cryogenic temperatures. Nat Commun. 2016;7(1):1. https://doi.org/10.1038/ncomms10602.
[21] Dingfeng X, Wang M, Li T, Wei X, Yiping L. A critical review of the mechanical properties of CoCrNi-based medium-entropy alloys. Microstructures. 2022. https://doi.org/10.20517/microstructures.2021.10.
[22] Gao P, Ma ZH, Gu J, Ni S, Suo T, Li YL, Song M, Mai YW, Liao XZ. Exceptional high-strain-rate tensile mechanical properties in a CrCoNi medium-entropy alloy. Sci China Mater. 2022;65:811. https://doi.org/10.1007/s40843-021-1798-6.
[23] Gludovatz B, Hohenwarter A, Catoor D, Chang EH, George EP, Ritchie RO. A fracture-resistant high-entropy alloy for cryogenic applications. Science. 2014;345(6201):1153. https://doi.org/10.1126/science.1254581.
[24] Niu SZ, Kou HC, Wang J, Li JS. Improved tensile properties of $Al_{0.5}$CoCrFeNi high-entropy alloy by tailoring microstructures. Rare Met. 2021;40(9):2508. https://doi.org/10.1007/s12598-016-0860-y.
[25] Qiu XW, Zhang YP, He L, Liu CG. Microstructure and corrosion resistance of AlCrFeCuCo high entropy alloy. J Alloys Compd. 2013;549:195. https://doi.org/10.1016/j.jallcom.2012.09.091.
[26] Zhu BH, Qiu HC, Jiang W, Yu QH. Oxidation behavior of $Al_{0.2}$CoCrFeNi high-entropy alloy film in supercritical water environment. Rare Met. 2022;41:1217. https://doi.org/10.1007/s12598-021-01859-1.
[27] Cantor B, Chang ITH, Knight P, Vincent AJB. Microstructural development in equiatomic multicomponent alloys. Mater Sci Eng A. 2004;375–377:213. https://doi.org/10.1016/j.msea.2003.10.257.
[28] Huang PK, Yeh JW, Shun TT, Chen SK. Multi-principal-element alloys with improved oxidation and wear resistance for thermal spray coating. Adv Eng Mater. 2004;6(1–2):74. https://doi.org/10.1002/adem.200300507.
[29] Ranganathan S. Alloyed pleasures: multimetallic cocktails. Curr Sci. 2003;85(10):1404.
[30] Song HQ, Tian FY, Hu QM, Vitos L, Wang YD, Shen J, Chen NX. Local lattice distortion in high-entropy alloys. Phys Rev Mater. 2017;1(2):023404. https://doi.org/10.1103/PhysRevMaterials.1.023404.
[31] Huang ZY, Dai YQ, Li Z, Zhang GQ, Chang CT, Ma J. Investigation on surface morphology and crystalline phase deformation of $Al_{80}Li_5Mg_5Zn_5Cu_5$ high-entropy alloy by ultra-precision cutting. Mater Des. 2020;186:108367. https://doi.org/10.1016/j.matdes.2019.108367.
[32] Zhang L, Hashimoto T, Yan JW. Machinability exploration for high-entropy alloy FeCrCoMnNi by ultrasonic vibration-assisted diamond turning. CIRP Ann. 2021;70(1):37. https://doi.org/10.1016/j.cirp.2021.04.090.
[33] Shen QK, Kong XD, Chen XZ. Fabrication of bulk Al-Co-Cr-Fe-Ni high-entropy alloy using combined cable wire arc additive manufacturing (CCW-AAM): microstructure and mechanical properties. J Mater Sci Technol. 2021;74:136. https://doi.org/10.1016/j.jmst.2020.10.037.
[34] Peng SY, Mooraj S, Feng R, Liu L, Ren J, Liu YF, Kong FY, Xiao ZY, Zhu C, Liaw PK, Chen W. Additive manufacturing of three-dimensional (3D)-architected CoCrFeNiMn high-entropy alloy with great energy absorption. Scr Mater. 2021;190:46. https://doi.org/10.1016/j.scriptamat.2020.08.028.
[35] Liu B, Raabe D, Eisenlohr P, Roters F, Arsenlis A, Hommes G. Dislocation interactions and low-angle grain boundary strengthening. Acta Mater. 2011;59(19):125. https://doi.org/10.1016/j.actamat.2011.07.067.
[36] Jiao ZM, Ma SG, Chu MY, Yang HJ, Wang ZH, Zhang Y, Qiao JW. Superior mechanical properties of $AlCoCrFeNiTi_x$ high-entropy alloys upon dynamic loading. J Mater Eng Perform. 2016;25(2):451. https://doi.org/10.1007/s11665-015-1869-3.
[37] Wang BF, Wang C, Liu B, Zhang XY. Dynamic mechanical properties and microstructure of an $(Al_{0.5}CoCrFeNi)_{0.95}Mo_{0.025}C_{0.025}$ high entropy alloy. Entropy. 2019;21(12):1154. https://doi.org/10.3390/e21121154.
[38] Ma Y, Yuan FP, Yang MX, Jiang P, Ma E, Wu XL. Dynamic shear deformation of a CrCoNi medium-entropy alloy with heterogeneous grain structures. Acta Mater. 2018;148:407. https://doi.org/10.1016/j.actamat.2018.02.016.
[39] Park JM, Moon J, Bae JW, Jang MJ, Park J, Lee S, Kim HS. Strain rate effects of dynamic compressive deformation on mechanical properties and microstructure of CoCrFeMnNi high-entropy alloy. Mater Sci Eng A. 2018;719:155. https://doi.org/10.1016/j.msea.2018.02.031.
[40] He JY, Wang Q, Zhang HS, Dai LD, Mukai T, Wu Y, Liu XJ, Wang H, Nieh TG, Lu ZP. Dynamic deformation behavior of a face-centered cubic FeCoNiCrMn high-entropy alloy. Sci Bull. 2018;63(6):362. https://doi.org/10.1016/j.scib.2018.01.022.
[41] Zaddach AJ, Niu C, Koch CC, Irving DL. Mechanical properties and stacking fault energies of NiFeCrCoMn high-entropy alloy. JOM. 2013;65(12):1780. https://doi.org/10.1007/s11837-013-0771-4.
[42] Stepanov N, Tikhonovsky M, Yurchenko N, Zyabkin D, Klimova M, Zherebtsov S, Efimov A, Salishchev G. Effect of cryo-deformation on structure and properties of CoCrFeNiMn high-entropy alloy. Intermetallics. 2015;59:8. https://doi.org/10.1016/j.intermet.2014.12.004.
[43] Li Z, Li X, Huang ZY, Zhang ZX, Liang X, Liu H, Liaw PK, Ma J, Shen J. Ultrasonic-vibration-enhanced plasticity of an entropic alloy at room temperature. Acta Mater. 2021;225:117569. https://doi.org/10.1016/j.actamat.2021.117569.
[44] Gu P, Dao M, Zhu YT. Strengthening at nanoscaled coherent twin boundary in fcc metals. Philos Mag. 2014;94(11):1249. https://doi.org/10.1080/14786435.2014.885138.
[45] Wen WX, Huang ZY, Li Z, Fu JN, Ruan WQ, Ren S, Zhang ZX, Liang X, Ma J. Multi-scale cold embossing of CoCrFeNiMn high entropy alloy with ultra-high temperature durability. Appl Mater Today. 2021;25:101233. https://doi.org/10.1016/j.apmt.2021.101233.